Progress In Electromagnetics Research, Vol. 168, 73–86, 2020

Radiation Gauge Potential-Based Time Domain Integral Equations for Penetrable Regions

Thomas E. Roth[1, 2] and Weng C. Chew[2, 3, *]

Abstract—Potential-based integral equations are being explored to develop numerical methods that avoid low frequency breakdown issues and are better suited to couple to quantum physics computations. Important classes of quantum electrodynamics problems are typically formulated in the radiation gauge, leading to interest in efficient numerical solutions able to be performed directly in this gauge. This work presents time domain integral equations for penetrable regions that are developed in the radiation gauge. An appropriate marching-on-in-time discretization scheme is developed that fully conforms to the spatial and temporal Sobolev space properties of the integral equations. It is shown that following this approach leads to a discrete system with improved stability properties that produces accurate results down to very low frequencies. The accuracy and stability of this formulation at low frequencies are shown through numerical results.

1. INTRODUCTION

Many semiclassical and quantum electrodynamics problems are formulated in the radiation gauge so that the scalar potential does not need to be considered [1, 2]. In many of these applications, computational electromagnetics (CEM) methods operating purely in the classical regime can be leveraged to supply the necessary information about the electromagnetic effects to the quantum calculation [3, 4]. Typically, this can be done by computing components of the *classical* dyadic Green's function for the electromagnetic environment by solving appropriately defined scattering problems. For instance, it was shown in [3] how the dynamics of atom-photon interactions can be solved in a general electromagnetic environment by computing the imaginary part of the dyadic Green's function. Although a different application, it was shown in [4] how the Casimir force between two objects could be evaluated using the same information provided by the dyadic Green's function for the electromagnetic environment being analyzed. Both of these applications have the electromagnetic field quantized, yet classical CEM can still play a vital role in studying these physical systems.

Despite this connection to classical CEM, these and other quantum applications stress the capability of many CEM methods. For instance, many quantum applications can require the analysis of large geometries with fine features composed of conducting and penetrable regions over extremely broad bandwidths [5–7]. One approach to meeting the needs of these emerging areas is with time domain integral equations (TDIEs), which can analyze large bandwidths in a single simulation and can also be accelerated with fast algorithms to handle large problems [8, 9]. Despite these favorable properties, TDIEs in electromagnetics suffer from low frequency and dense mesh breakdowns, impacting their ability to perform extremely broadband analyses of complicated structures efficiently [10, 11].

The low frequency and dense mesh breakdowns of traditional TDIEs are primarily consequences of the spectral properties (in the Hilbert space sense) of the hypersingular integral operators that

Received 28 July 2020, Accepted 10 October 2020, Scheduled 15 October 2020
* Corresponding author: Weng C. Chew (wcchew@purdue.edu).
[1] Sandia National Laboratories, USA. [2] Department of Electrical and Computer Engineering, University of Illinois at Urbana-Champaign, USA. [3] School of Electrical and Computer Engineering, Purdue University, USA.

are present in many electromagnetic integral equations [11]. For example, this operator is present in the electric field integral equation (EFIE) for perfect electric conductors, as well as most penetrable formulations.

Early approaches at overcoming the issue of low frequency breakdown mainly involved performing quasi-Helmholtz decompositions of the current densities, such as a loop-tree decomposition [10]. Efforts to address the dense mesh breakdown have primarily focused on developing preconditioners, with the most successful being the Calderón preconditioners that leverage the self-regularizing properties of the hypersingular integral operator [11]. Although successful, the combination of these approaches requires the construction of the spatial basis functions for the quasi-Helmholtz decomposition, which can be difficult to perform efficiently for complex objects [12].

Alternative approaches to addressing the low frequency breakdown that result in simpler discretization schemes have also been pursued. These include the augmented EFIE and current and charge integral equation (CCIE) formulations. These separate the hypersingular integral operator into two parts that can be stably discretized by treating the surface charge densities as additional sets of unknowns to the surface current densities [12, 13]. Preconditioning these equations can be pursued to improve convergence issues that may remain due to dense mesh breakdown effects [12].

A more recent approach to addressing low frequency breakdown issues is to develop equations directly in terms of electromagnetic potentials, as opposed to fields [14–16]. These systems naturally do not exhibit low frequency breakdown effects, and have shown promise. However, all potential-based systems have been formulated in the Lorenz gauge so far, leaving a gap for handling applications more naturally expressed in the radiation gauge. For instance, both the atom-photon interaction and Casimir force calculations discussed in [3, 4] can be viewed as being quantized in the radiation gauge. Although it is in principle possible to recover results in the radiation gauge from a solver operating in the Lorenz gauge, implementing these gauge transformations as a post-processing step can be complicated and inefficient. Hence, having appropriate solvers developed directly in the radiation gauge can be of interest for these applications.

As a result, this work develops TDIEs for penetrable regions in the radiation gauge that do not exhibit a low frequency breakdown. These TDIEs are derived in Section 2, and are seen to be similar to the CCIE [13], which to the authors' best knowledge has never been demonstrated in the time domain. To assist in discretizing the system, the spatiotemporal Sobolev space properties of the integral operators are discussed [17]. To aid in interpreting the spatiotemporal Sobolev space properties discussed, a short primer on these spaces is included in the appendix. Following this, Section 3 presents a discretization that fully conforms to the Sobolev space properties of the integral operators, enhancing the stability of the system. Section 4 then presents numerical results that demonstrate the stability and accuracy of this formulation down to very low frequencies.

2. FORMULATION

In this section, potential-based TDIEs for penetrable regions are derived in the radiation gauge. To do this, traces of the integral representation of solutions to the radiation gauge wave equation are introduced in Section 2.1. Following this, the spatiotemporal Sobolev space properties of these traces are discussed in Section 2.2 to assist in discretizing the integral equation system presented in Section 2.3.

2.1. Vector Potential Traces in the Radiation Gauge

To derive integral equations, the differential equations the potentials obey must be found. To do this, the potentials are introduced in the standard way so that Maxwell's equations are satisfied [18]. The particular gauge often used in quantum problems is the radiation gauge, which is characterized by $\Phi = 0$ and $\nabla \cdot \mathbf{A} = 0$ (this is also sometimes referred to as the $\Phi = 0$ gauge). This gauge is typically used when no near-field sources are present, but also applies when only divergence-free current densities are considered [1, 18]. For this situation, only the wave equation for the vector potential needs to be considered. For deriving an integral representation formula, the source-free wave equation can be used, which is

$$\nabla \times \nabla \times \mathbf{A} + \mu\epsilon\partial_t^2 \mathbf{A} = 0. \tag{1}$$

This equation has an identical form to that for electromagnetic fields, so the standard Stratton-Chu integral representation formula can be easily adapted to the current case [19]. However, for increased clarity, the radiation gauge integral representation formula will be developed explicitly in this work.

The simplest way to establish the desired radiation gauge integral representation formula is to use the scalar-vector Green's theorem [20, 21]. This is

$$\int_V \Big[b\big(\nabla\times\nabla\times\mathbf{a}\big) + \mathbf{a}\nabla^2 b + \big(\nabla\cdot\mathbf{a}\big)\nabla b \Big] dV = -\int_S \Big[\big(\hat{n}\cdot\mathbf{a}\big)\nabla b + (\hat{n}\times\mathbf{a})\times\nabla b + \big(\hat{n}\times\nabla\times\mathbf{a}\big) b \Big] dS, \quad (2)$$

where $\hat{n}$ is the unit normal vector pointing into the volume V. Further, b and $\mathbf{a}$ are arbitrary scalar and vector functions, respectively. The only conditions required of b and $\mathbf{a}$ for Rq. (2) to be valid are that they have the necessary continuity properties for the derivatives in Eq. (2) to be meaningfully evaluated [20].

It is easiest to use this identity in the frequency domain and to then transform the results back to the time domain. Considering this, a frequency domain radiation gauge integral representation formula can be developed by setting $\mathbf{a} = \tilde{\mathbf{A}}(\mathbf{r}')$ and $b = \tilde{g}(\mathbf{r},\mathbf{r}')$ in Eq. (2), where a tilde denotes a quantity is in the frequency domain with angular frequency ω and $\tilde{g}$ is the free-space Green's function. In the frequency domain, Eq. (1) becomes

$$\nabla\times\nabla\times\tilde{\mathbf{A}} - \mu\epsilon\omega^2\tilde{\mathbf{A}} = 0 \quad (3)$$

and the Green's function can be seen to obey [20]

$$\nabla^2\tilde{g}(\mathbf{r},\mathbf{r}') + \mu\epsilon\omega^2\tilde{g}(\mathbf{r},\mathbf{r}') = -\delta(\mathbf{r}-\mathbf{r}'). \quad (4)$$

To use Eq. (2), it will be advantageous to have S be a surface bounding a particular region in space (e.g., the surface of a scatterer) and to have V stretch from S to infinity. The additional surface integral that would occur at infinity for this setup vanishes due to the radiation condition, and so can be ignored [21, 22]. At this point, $\tilde{\mathbf{A}}$ and $\tilde{g}$ can be substituted into Eq. (2). The resulting expression can then be simplified by using Eqs. (3) and (4) to arrive at

$$\int_V \Big[\big(\nabla'\cdot\tilde{\mathbf{A}}\big)\nabla'\tilde{g} - \tilde{\mathbf{A}}\delta(\mathbf{r}-\mathbf{r}') \Big] dV' = -\int_S \Big[\tilde{g}\big(\hat{n}'\times\nabla'\times\tilde{\mathbf{A}}\big) - \nabla\tilde{g}\big(\hat{n}'\cdot\tilde{\mathbf{A}}\big) + \nabla\times\big(\tilde{g}\hat{n}'\times\tilde{\mathbf{A}}\big) \Big] dS'. \quad (5)$$

Noting that $\nabla'\cdot\mathbf{A} = 0$ due to the gauge condition, the volume integral can be evaluated to give

$$\tilde{\mathbf{A}}(\mathbf{r}) = \int_S \Big[\tilde{g}\big(\hat{n}'\times\nabla'\times\tilde{\mathbf{A}}\big) - \nabla\tilde{g}\big(\hat{n}'\cdot\tilde{\mathbf{A}}\big) + \nabla\times\big(\tilde{g}\hat{n}'\times\tilde{\mathbf{A}}\big) \Big] dS', \ \ \mathbf{r}\notin S, \quad (6)$$

which is the desired integral representation formula.

The time domain integral representation formula can now be derived by taking the inverse Fourier transform of Eq. (6). After redefining the surface sources, this gives

$$\mathbf{A}(\mathbf{r},t) = \mu\int_S \frac{\mathbf{j}(\mathbf{r}',\tau)}{4\pi R} dS' - \nabla\int_S \frac{\partial_t^{-1}\mathrm{d}(\mathbf{r}',\tau)}{4\pi R\epsilon} dS' + \nabla\times\int_S \frac{\partial_t^{-1}\mathbf{m}(\mathbf{r}',\tau)}{4\pi R} dS', \ \ \mathbf{r}\notin S, \quad (7)$$

where $\mathbf{j} = \mu^{-1}\hat{n}'\times\nabla'\times\mathbf{A}$, $\mathrm{d} = \hat{n}'\cdot\epsilon\partial_t\mathbf{A}$, and $\mathbf{m} = \hat{n}'\times\partial_t\mathbf{A}$. Further, $\tau = t - R/c$ and ∂_t^{-1} denotes a time integration from $-\infty$ to the temporal argument of the function it is applied to. Note that the reasons for the temporal rescaling of the surface sources in Eq. (7) will be discussed in Section 2.2.

Before continuing, it is useful to comment on the physical interpretation of the sources introduced in Eq. (7), since they are somewhat unfamiliar when written in this potential-based form. Considering that in the radiation gauge $\mathbf{B} = \nabla\times\mathbf{A}$ and $\mathbf{E} = -\partial_t\mathbf{A}$, it can be seen that $\mathbf{j}$ and $\mathbf{m}$ correspond to equivalent electric and magnetic current densities, respectively. Similarly, d can be identified as an electric charge density which obeys a continuity equation with $\mathbf{j}$. This can be established by taking the divergence of $\mathbf{j}$ and using Eq. (1).

Typically, integral equations are formulated after using the continuity equation to eliminate d from Eq. (7). This will not be done in this work because it introduces a hypersingular integral operator in Eq. (7), damaging the low frequency performance. Retaining d as a surface source follows the core idea of the augmented EFIE and CCIE, and results in an integral representation that is stable down to very low frequencies [12, 13].

To form integral equations, traces of the vector potential, as defined through Eq. (7), need to be determined for the limit as $\mathbf{r}$ approaches S. Note that a *trace* in this context refers to *trace operators* from the theory of Sobolev spaces. For the purposes of this work, these can simply be viewed as a way to define functions on surfaces as boundary values of functions defined throughout a volume. A simple example is $\hat{n} \times \mathbf{F}$, where $\hat{n}$ is a normal unit vector on a surface S and $\mathbf{F}$ is some vector function defined throughout the volume of interest. Although this simple view is acceptable for this work, a more sophisticated consideration is necessary to rigorously establish stability properties of TDIEs that are central to our discretization approach that will be detailed in Section 3 [17, 23].

Of particular interest are traces related to boundary conditions enforcing the continuity of the tangential components of the electric and magnetic fields and the normal components of the electric and magnetic fluxes. For instance, the trace corresponding to the normal component of the electric flux can be written as $\hat{n} \cdot \epsilon \partial_t \mathbf{A}\{\mathbf{j}, \mathrm{d}, \mathbf{m}\}(\mathbf{r}, t)$, where the notation emphasizes that this is a functional evaluated at position $\mathbf{r}$ and time t that depends on the source functions given in the braces. The explicit form of this trace can be found by plugging Eq. (7) into this expression for $\mathbf{A}$ and then taking the limit as $\mathbf{r}$ approaches S. Considering this, the explicit form of the traces that are of interest to this work are

$$\hat{n}\times\big[\partial_t \mathbf{A}_j\{\mathbf{j},\mathrm{d},\mathbf{m}\}(\mathbf{r},t)\big]\times\hat{n} = \mu_j \partial_t \mathcal{T}_j\{\mathbf{j}\}(\mathbf{r},t) - \epsilon_j^{-1}\nabla\mathcal{S}_j\{\mathrm{d}\}(\mathbf{r},t) \pm \frac{1}{2}\hat{n}\times\mathbf{m}(\mathbf{r},t) - \mathcal{K}_j\{\mathbf{m}\}(\mathbf{r},t), \tag{8}$$

$$\hat{n}\cdot\epsilon_j \partial_t \mathbf{A}_j\{\mathbf{j},\mathrm{d},\mathbf{m}\}(\mathbf{r},t) = \mu_j\epsilon_j\hat{n}\cdot\partial_t\mathcal{T}_j\{\mathbf{j}\}(\mathbf{r},t) \pm \frac{1}{2}\mathrm{d}(\mathbf{r},t) + \mathcal{N}_j\{\mathrm{d}\}(\mathbf{r},t) + \hat{n}\cdot\epsilon_j\nabla\times\mathcal{T}_j\{\mathbf{m}\}(\mathbf{r},t), \tag{9}$$

$$\hat{n}\times\big[\mu_j^{-1}\nabla\times\mathbf{A}_j\{\mathbf{j},\mathbf{m},\mathrm{b}\}(\mathbf{r},t)\big]\times\hat{n} = -\epsilon_j\partial_t\mathcal{T}_j\{\mathbf{m}\}(\mathbf{r},t) + \mu_j^{-1}\nabla\mathcal{S}_j\{\mathrm{b}\}(\mathbf{r},t) \pm \frac{1}{2}\hat{n}\times\mathbf{j}(\mathbf{r},t) - \mathcal{K}_j\{\mathbf{j}\}(\mathbf{r},t), \tag{10}$$

$$\hat{n}\cdot\nabla\times\mathbf{A}_j\{\mathbf{j},\mathbf{m},\mathrm{b}\}(\mathbf{r},t) = -\mu_j\epsilon_j\hat{n}\cdot\partial_t\mathcal{T}_j\{\mathbf{m}\}(\mathbf{r},t) \mp \frac{1}{2}\mathrm{b}(\mathbf{r},t) - \mathcal{N}_j\{\mathrm{b}\}(\mathbf{r},t) + \hat{n}\cdot\mu_j\nabla\times\mathcal{T}_j\{\mathbf{j}\}(\mathbf{r},t), \tag{11}$$

where $\mathrm{b} = -\hat{n}' \cdot \nabla \times \mathbf{A}$, i.e., an equivalent magnetic charge density related to $\mathbf{m}$ through a continuity equation. Further aspects of the notation include the subscript j, which is used to differentiate whether the limit is approaching S from the exterior (e) or interior (i) regions. Note that the top (bottom) sign for the Cauchy principal value terms should be selected for the limit being taken from the exterior (interior) region.

The integral operators used in Eqs. (8) to (11) are

$$\mathcal{T}_j\{\mathbf{q}\}(\mathbf{r},t) = \int_S \frac{\mathbf{q}(\mathbf{r}',\tau_j)}{4\pi R} dS', \tag{12}$$

$$\mathcal{K}_j\{\mathbf{q}\}(\mathbf{r},t) = \int_S \hat{R}\times\left[\frac{\mathbf{q}(\mathbf{r}',\tau_j)}{4\pi R^2} + \frac{\partial_t\mathbf{q}(\mathbf{r}',\tau_j)}{4\pi R c_j}\right] dS', \tag{13}$$

$$\mathcal{S}_j\{p\}(\mathbf{r},t) = \int_S \frac{p(\mathbf{r}',\tau_j)}{4\pi R} dS', \tag{14}$$

$$\mathcal{N}_j\{p\}(\mathbf{r},t) = \int_S \hat{n}\cdot\hat{R}\left[\frac{p(\mathbf{r}',\tau_j)}{4\pi R^2} + \frac{\partial_t p(\mathbf{r}',\tau_j)}{4\pi R c_j}\right] dS'. \tag{15}$$

where $\hat{R}$ is a unit vector pointing in the direction from $\mathbf{r}'$ to $\mathbf{r}$. Note that $\mathcal{K}_j$ and $\mathcal{N}_j$ should be evaluated in the Cauchy principal value sense.

2.2. Sobolev Spaces

Sobolev spaces form a central part of understanding the mathematical properties of integral operators, and can be vital in developing well-performing discretizations [24]. Along these lines, it is essential for basis and testing functions to be selected from appropriate Sobolev spaces to achieve a stable marching-on-in-time (MOT) discretization of systems combining vector and scalar TDIEs [17]. In particular, basis functions are selected from the domain space of the integral operators, while testing functions are selected from the dual to the range space of the integral operators [25]. To support this, the Sobolev space properties of Eqs. (8) to (11) are discussed in this section. The details of the analysis to determine the properties presented in this section can be found in [17, 23, 26].

To begin, we briefly introduce the notation for the family of spatiotemporal Sobolev spaces used. More details on these spaces can be found in [17] and the appendix of this work. The space of div-conforming functions is denoted as $\mathscr{H}_{\text{div}}^{s_1,s_2}$, where s_1 (s_2) gives the temporal (spatial) order of the Sobolev space. Similarly, the space of curl-conforming functions is denoted by $\mathscr{H}_{\text{curl}}^{s_1,s_2}$, and spaces for scalar functions are denoted by $\mathcal{H}^{s_1,s_2}$. Note that for a function to be a member of a higher order Sobolev space requires the function to be smoother (i.e., more derivatives can be taken of it). As a result, taking a derivative of a function will lower its Sobolev space order, while integrating a function can raise its Sobolev space order.

As alluded to above, developing a well-performing discretization will require knowing the dual spaces for all of the spatiotemporal Sobolev spaces discussed. The dual spaces are summarized as: $\left(\mathscr{H}_{\text{div}}^{s_1,s_2}\right)^* = \mathscr{H}_{\text{curl}}^{-s_1,s_2}$, $\left(\mathscr{H}_{\text{curl}}^{s_1,s_2}\right)^* = \mathscr{H}_{\text{div}}^{-s_1,s_2}$, and $\left(\mathcal{H}^{s_1,s_2}\right)^* = \mathcal{H}^{-s_1,-s_2}$; where for a Sobolev space H, the dual space is denoted as H^*.

The largest Sobolev space that each source is a member of can be found through the functional analysis of Eqs. (8) to (11). The results of this analysis give $\mathbf{j}, \mathbf{m} \in \mathscr{H}_{\text{div}}^{1/2,-1/2}$ and $\mathrm{d}, \mathrm{b} \in \mathcal{H}^{1/2,-1/2}$. From this, it is seen that the temporal Sobolev space order for each function is the same. This is due to a deliberate choice in the definitions of the various source terms. For example, if instead of d we had elected to use as a source $\mathrm{d}' = \hat{n}' \cdot \epsilon\mathbf{A}$, the temporal order of the Sobolev spaces for d' would be different from the rest of the sources. Typically it is convenient to define all the sources so that they have the same temporal Sobolev space order, since this allows the same temporal basis function to be used for all sources in an MOT discretization [17]. However, for some potential-based formulations it can be more advantageous to have some sources with different temporal Sobolev space orders, as was done in [27].

To determine the range space of the integral operators in Eqs. (12) to (15), we note their mapping properties. These are

$$\mathcal{T}_j : \mathscr{H}_{\text{div}}^{s,-1/2} \to \mathscr{H}_{\text{curl}}^{s+2,-1/2}, \tag{16}$$

$$\mathcal{K}_j : \mathscr{H}_{\text{div}}^{s,-1/2} \to \mathscr{H}_{\text{curl}}^{s+1,-1/2}, \tag{17}$$

$$\mathcal{S}_j : \mathcal{H}^{s,-1/2} \to \mathcal{H}^{s+2,1/2}, \tag{18}$$

$$\mathcal{N}_j : \mathcal{H}^{s,-1/2} \to \mathcal{H}^{s+1,-1/2}. \tag{19}$$

Note that the increase of the temporal Sobolev space order of $\mathcal{T}_j$ and $\mathcal{S}_j$ are higher than that for $\mathcal{K}_j$ and $\mathcal{N}_j$. This is due to the spatial derivatives implied in $\mathcal{K}_j$ and $\mathcal{N}_j$, which impact the temporal order of the integral operators [17]. This difference is balanced out in Eqs. (8) to (11), where a spatial or temporal derivative is applied to every instance of $\mathcal{T}_j$ and $\mathcal{S}_j$. It is important to recognize that for Sobolev spaces of electromagnetic functions, spatial derivatives also impact the temporal order of the Sobolev spaces [17]. This can be intuitively understood from the structure of Maxwell's equations where $\mathbf{E}$ and $\mathbf{H}$ are dual to each other. As a result, it would be expected for them to generally be members of the same Sobolev space. Considering either of Maxwell's curl equations, it is immediately seen that for all the functions of these equations to be in the same Sobolev space the spatial derivative will necessarily impact the temporal Sobolev space order.

The range spaces of Eqs. (8) to (11) can now be found using Eqs. (16) to (19). Performing this, we see that the range space of Eqs. (8) and (10) is $\mathscr{H}_{\text{curl}}^{3/2,-1/2}$. Similarly, the range space of Eqs. (9) and (11) is $\mathcal{H}^{3/2,-1/2}$. From this, it can be seen that the traces given in Eqs. (8) to (11) were selected so that the temporal order of the range spaces would be the same, and equal to 3/2. This was done for two reasons. The first is that it is essential for the range spaces to all have the same temporal Sobolev space order to achieve a stable MOT discretization [17]. Secondly, having the temporal order equal to 3/2 is advantageous so that the temporal dual space has order $-3/2$, which is the highest order space that contains the Dirac delta function. As a result, a MOT discretization naturally conforms to the Sobolev space properties of Eqs. (8) to (11) if a correct temporal basis function is selected [17].

Although this is the approach taken in this work, it is also possible to consider other traces of the vector potential, e.g., $\hat{n}\times[\mathbf{A}_j\{\mathbf{j}, \mathrm{d}, \mathbf{m}\}(\mathbf{r}, t)]\times\hat{n}$. This leads to integral equations with a different temporal range space, which requires a different set of basis functions to discretize using a MOT approach [16, 17]. The properties of an integral equation system using these other traces in the radiation gauge can be

considered in future work.

2.3. Radiation Gauge Integral Equation System

To derive an explicit set of integral equations, a two region problem with an incident field only in the exterior region will be considered. This is schematically shown in Fig. 1, where $\mathbf{A}_{\text{inc}}$ is assumed to be produced by a source that is compatible with the radiation gauge. To form the complete system for the four surface unknowns, we use a Müeller-inspired combination of auxiliary exterior and interior integral equations derived using the traces given in Eqs. (8) to (11) [28]. For each equation, this corresponds to a simple rearrangement of the boundary condition enforcing the continuity of the electromagnetic fields and fluxes. For instance,

$$\hat{n}\times\big[\partial_t\mathbf{A}_e\{\mathbf{j},\mathrm{d},\mathbf{m}\}(\mathbf{r},t)\big]\times\hat{n}-\hat{n}\times\big[\partial_t\mathbf{A}_i\{\mathbf{j},\mathrm{d},\mathbf{m}\}(\mathbf{r},t)\big]\times\hat{n}=-\hat{n}\times\big[\partial_t\mathbf{A}_{\text{inc}}(\mathbf{r},t)\big]\times\hat{n},\ \ \mathbf{r}\in S, \tag{20}$$

can be seen as enforcing that the tangential electric field is continuous across S by noting that $\hat{n}\times[\partial_t\mathbf{A}_{e(i)}\{\mathbf{j},\mathrm{d},\mathbf{m}\}(\mathbf{r},t)]\times\hat{n}$ is the scattered potential in the exterior (interior) region. The benefit of combining traces in this way is that the resulting matrix system will have an identity operator along the diagonal, which improves the conditioning of the discretized matrix system.

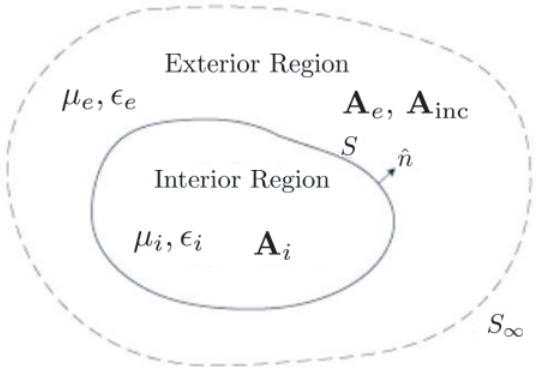

Figure 1. Configuration of the two-region problem considered in this work.

The remaining equations for the integral equation system are

$$\hat{n}\cdot\epsilon_e\partial_t\mathbf{A}_e\{\mathbf{j},\mathrm{d},\mathbf{m}\}(\mathbf{r},t)-\hat{n}\cdot\epsilon_i\partial_t\mathbf{A}_i\{\mathbf{j},\mathrm{d},\mathbf{m}\}(\mathbf{r},t)=-\hat{n}\cdot\epsilon_e\partial_t\mathbf{A}_{\text{inc}}(\mathbf{r},t),\ \ \mathbf{r}\in S, \tag{21}$$

$$\hat{n}\times\big[\mu_e^{-1}\nabla\times\mathbf{A}_e\{\mathbf{j},\mathbf{m},\mathrm{b}\}(\mathbf{r},t)\big]\times\hat{n}-\hat{n}\times\big[\mu_i^{-1}\nabla\times\mathbf{A}_i\{\mathbf{j},\mathbf{m},\mathrm{b}\}(\mathbf{r},t)\big]\times\hat{n}=-\hat{n}\times\big[\mu_e^{-1}\nabla\times\mathbf{A}_{\text{inc}}(\mathbf{r},t)\big]\times\hat{n},\ \ \mathbf{r}\in S, \tag{22}$$

$$\hat{n}\cdot\nabla\times\mathbf{A}_e\{\mathbf{j},\mathbf{m},\mathrm{b}\}(\mathbf{r},t)-\hat{n}\cdot\nabla\times\mathbf{A}_i\{\mathbf{j},\mathbf{m},\mathrm{b}\}(\mathbf{r},t)=-\hat{n}\cdot\nabla\times\mathbf{A}_{\text{inc}}(\mathbf{r},t),\ \ \mathbf{r}\in S. \tag{23}$$

Utilizing all of the boundary conditions in this way ensures the low frequency accuracy of the overall integral equation system. This occurs because Eqs. (20) to (23) naturally decouple into electrostatic and magnetostatic integral equations as the frequency lowers [13].

It is important to note that the main way this integral equation system differs from the CCIE of [13] is in the vector equations. In particular, the original CCIE of [13] was implemented using *rotated* vector equations, i.e., it would correspond to equations built from traces of the form $\hat{n}\times\partial_t\mathbf{A}_j\{\mathbf{j},\mathrm{d},\mathbf{m}\}(\mathbf{r},t)$. Although this difference is subtle, by not utilizing rotated vector equations our discretization scheme leads to simpler numerical integrations that can leverage standard approaches for singularity extraction and transferring of spatial derivatives onto testing functions.

3. DISCRETIZATION

The discretization of Eqs. (20) to (23) is discussed in this section. To enhance the numerical stability of the system, a discretization that fully conforms to the spatiotemporal Sobolev space properties of these equations is developed.

To begin, we consider the temporal basis function, which significantly impacts the stability of a MOT system [17]. In general, the basis function for the MOT system needs to be selected so that the MOT discretization is *functionally equivalent* to one that directly matches the Sobolev space properties of the system being discretized [17]. However, in some special cases, the equations being discretized can be scaled such that a MOT discretization is the functionally correct discretization (i.e., it directly conforms to the Sobolev spaces of the system). This approach was taken in this work, as mentioned in Section 2.2, so that using a basis function from a Sobolev space with order 1/2 will result in a stable system. A function that meets these properties is a triangle function defined by

$$T(t) = \begin{cases} 1 - \dfrac{|t|}{\Delta t}, & \text{for } |t| \leq \Delta t \\ 0, & \text{elsewhere,} \end{cases} \tag{24}$$

where Δt is the width of the time step used in the simulation.

In contrast to the CCIE of [13], our spatial basis functions are selected to fully conform to the Sobolev space properties of the integral operators. The functions used are defined on the primal mesh, and a dual mesh formed by the barycentric refinement of the primal mesh. In all cases, the basis and testing functions have been selected in accordance with the results of [29], where functions on the dual mesh were carefully constructed to lead to good discretizations when combined with standard functions used on the primal mesh.

Considering the spatial domain spaces of Eqs. (16) and (17), it is seen that $\mathbf{j}$ and $\mathbf{m}$ should be discretized with div-conforming basis functions. In particular, $\mathbf{j}$ is discretized with a Rao-Wilton-Glisson (RWG) function, denoted by $\mathbf{f}_n$, where n is the index of a primal mesh edge [30]. To ensure every integral operator can be tested well, it is necessary to use a different div-conforming basis function to discretize $\mathbf{m}$. A common approach to address this is to use a differential forms motivated discretization by using functions defined on the dual mesh for $\mathbf{m}$ [31]. Popular choices for this are the Chen-Wilton or Buffa-Christiansen (BC) functions [29, 32]. In this work, we use the BC function, denoted by $\mathbf{g}_n$, where n is the index of a primal mesh edge [29]. Although the BC function is associated with primal mesh edges, it is composed of a linear combination of RWG functions defined on the dual mesh (e.g., see [24, 29]).

Considering the spatial domain spaces given in Eqs. (18) and (19), it is seen that the two scalar unknowns should be discretized with spatial functions from the Sobolev space with order $-1/2$. For a function to be in this space, it must at least be a piecewise constant function (see the appendix for more details). Further, it is natural to have these functions defined on the same mesh as the vector unknown they are related to through a continuity equation (e.g., $\mathbf{j}$ and d are related). As a result, d is discretized with a piecewise constant function supported over a single primal mesh triangle, denoted by u_n, where n is the index of the primal mesh triangle. Similarly, b is discretized with a piecewise constant function whose support covers all dual mesh triangles attached to a single primal mesh node (illustrated in Fig. 2(a) and defined in [29]). This function is denoted by v_n, where n is the index of the primal mesh node the function is associated with.

Spatial testing functions are selected to have a square matrix system that fully conforms to the Sobolev space properties of the integral operators. Considering Eqs. (16) and (17), we see that Eqs. (20) and (23) should be tested with div-conforming functions. As a result, Eq. (20) is tested with RWG functions. For a trace from a single region and a particular combination of basis and testing functions, this yields

$$\langle \mathbf{f}_m, \partial_t \mathbf{A}_j\{\mathbf{f}_n, \mathrm{u}_k, \mathbf{g}_\ell\}\rangle = \langle \mathbf{f}_m, \mu_j \partial_t \mathcal{T}_j\{\mathbf{f}_n\}\rangle + \langle \nabla\cdot\mathbf{f}_m, \epsilon_j^{-1}\mathcal{S}_j\{\mathrm{u}_k\}\rangle \pm \frac{1}{2}\langle \mathbf{f}_m, \hat{n}\times\mathbf{g}_\ell\rangle - \langle \mathbf{f}_m, \mathcal{K}_j\{\mathbf{g}_\ell\}\rangle. \tag{25}$$

In Eq. (25),

$$\langle \mathbf{F}, \mathbf{G}\rangle = \int_S \mathbf{F}(\mathbf{r}, t)\cdot\mathbf{G}(\mathbf{r}, t) dS, \tag{26}$$

and a similar definition also applies for scalar integrals. Similarly, Eq. (23) is tested with BC functions, yielding

$$\langle \mathbf{g}_m, \nabla\times\mathbf{A}_j\{\mathbf{f}_n, \mathbf{g}_\ell, \mathrm{v}_k\}\rangle = -\langle \mathbf{g}_m, \epsilon_j \partial_t \mathcal{T}_j\{\mathbf{g}_\ell\}\rangle - \langle \nabla\cdot\mathbf{g}_m, \mu_j^{-1}\mathcal{S}_j\{\mathrm{v}_k\}\rangle \pm \frac{1}{2}\langle \mathbf{g}_m, \hat{n}\times\mathbf{f}_n\rangle - \langle \mathbf{g}_m, \mathcal{K}_j\{\mathbf{f}_n\}\rangle. \tag{27}$$

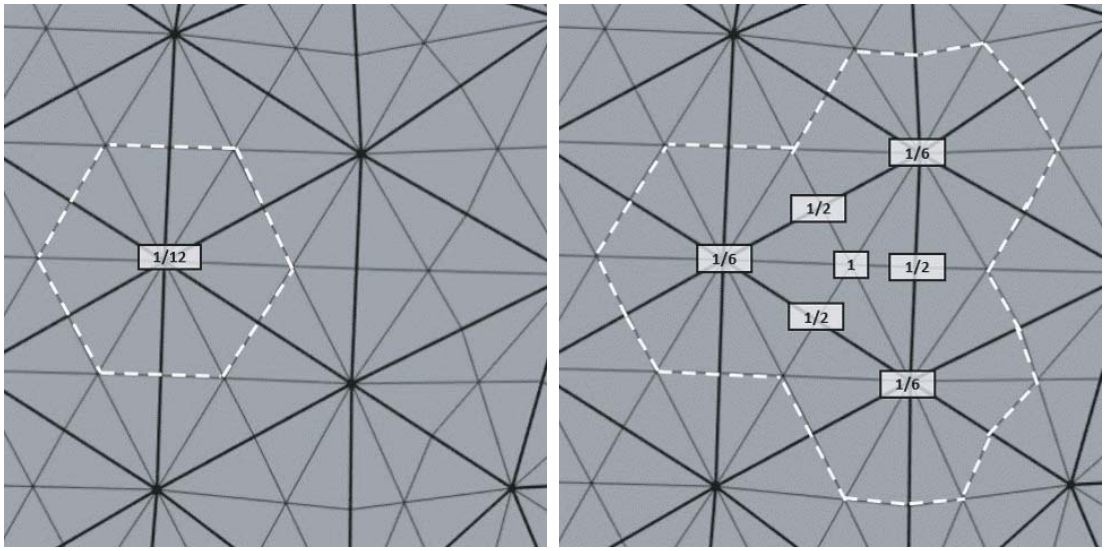

(a) (b)

Figure 2. Definitions of various spatial functions used in the discretization. Each function is composed of linear combinations of functions defined on the dual mesh. The support of the function is denoted by dashed lines. The numbers in boxes denote the scaling factors used in the linear combination for any function touching the box. Thicker lines denote edges on the primal mesh, while thinner lines denote edges on the dual mesh. Functions are (a) v_n made from piecewise constant functions and (b) ψ_n made from pyramid functions.

This testing approach ensures that the discretization of the rotated identity operators in these equations produces well-conditioned square matrices [29].

From Eq. (19), we see that the scalar equations (21) and (23) should be tested with a function from a spatial Sobolev space of order 1/2. That is, these functions should become piecewise constants after being differentiated. As a result, Eq. (23) is tested with a pyramid function associated with primal mesh nodes. The pyramid function is equal to 1 at the node it is associated with and varies linearly to 0 at all surrounding nodes. This function is denoted as φ_n, where n is the index of the primal mesh node the function is associated with. Using this function, the tested form of Eq. (23) is

$$\begin{aligned} &\langle \varphi_m, \hat{n} \cdot \nabla \times \mathbf{A}_j\{\mathbf{f}_n, \mathbf{g}_\ell, \mathrm{v}_k\}\rangle \\ &= -\langle \varphi_m, \mu_j \epsilon_j \hat{n} \cdot \partial_t \mathcal{T}_j\{\mathbf{g}_\ell\}\rangle \mp \frac{1}{2}\langle \varphi_m, \mathrm{v}_k\rangle - \langle \varphi_m, \mathcal{N}_j\{\mathrm{v}_k\}\rangle - \langle \hat{n} \times \nabla \varphi_m, \mu_j \mathcal{T}_j\{\mathbf{f}_n\}\rangle. \end{aligned} \tag{28}$$

Finally, Eq. (21) is tested with a function associated with primal mesh triangles, and is defined as a linear combination of pyramid functions defined on the dual mesh (illustrated in Fig. 2(b) and defined in [29]). This function is denoted by ψ_n, where n is the index of the primal mesh triangle the function is associated with. Using this function, the tested form of Eq. (21) is

$$\begin{aligned} &\langle \psi_m, \hat{n} \cdot \epsilon_j \partial_t \mathbf{A}_j\{\mathbf{f}_n, \mathrm{u}_k, \mathbf{g}_\ell\}\rangle \\ &= \langle \psi_m, \mu_j \epsilon_j \hat{n} \cdot \partial_t \mathcal{T}_j\{\mathbf{f}_n\}\rangle \pm \frac{1}{2}\langle \psi_m, \mathrm{u}_k\rangle + \langle \psi_m, \mathcal{N}_j\{\mathrm{u}_k\}\rangle - \langle \hat{n} \times \nabla \psi_m, \epsilon_j \mathcal{T}_j\{\mathbf{g}_\ell\}\rangle. \end{aligned} \tag{29}$$

As mentioned earlier, the combination of scalar basis and testing functions used in this work follows the careful construction of functions developed in [29]. The result of this is that the square matrices that arise from the discretization of the identity operators in Eqs. (21) and (23) are well-conditioned.

4. NUMERICAL RESULTS

Numerical results are presented to demonstrate the stability and accuracy of this system down to very low frequencies. Stability is assessed through an eigenvalue stability analysis of the MOT system, with

any eigenvalues lying outside the unit circle meaning that the system is unstable [33].

The first set of numerical examples are performed to highlight the importance of having basis and testing functions conform to the Sobolev space properties of the TDIEs. The object simulated is a one meter radius sphere with a relative permittivity of 2.56. The excitation is a plane wave with temporal variation defined by a modulated Gaussian pulse. The center frequency is 10 MHz, the bandwidth is 5 MHz, and the time step is 3.33 ns. The results of eigenvalue stability analyses for three different cases are shown in Fig. 3.

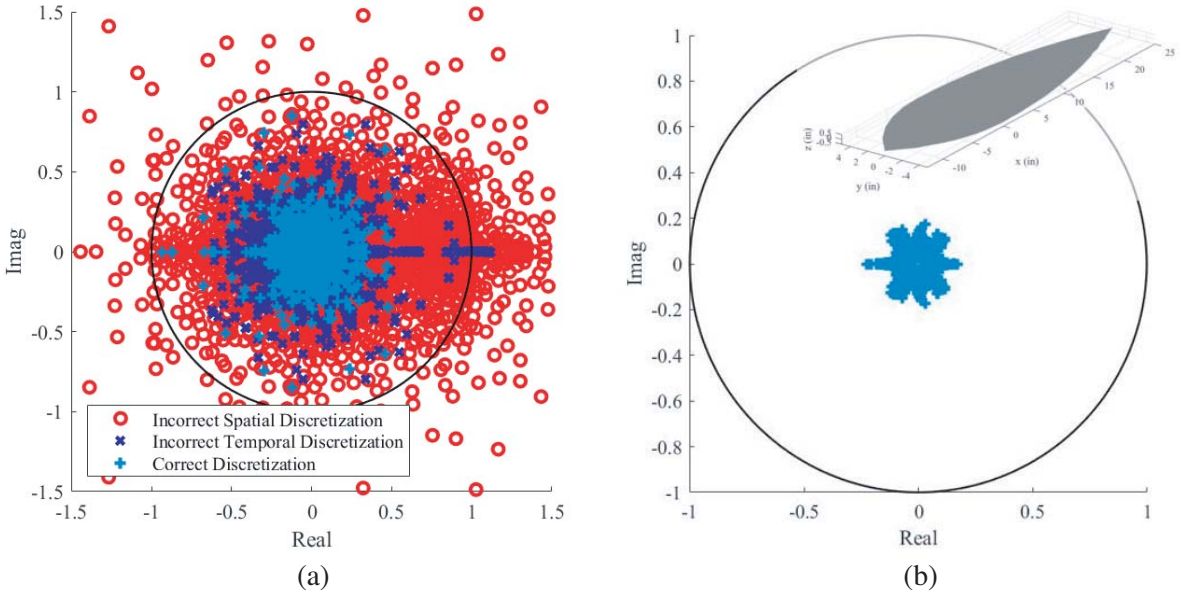

Figure 3. Stability results for (a) different discretization approaches for a sphere and (b) a conforming discretization of a thin double ogive.

The first case is for the discretization detailed in Section 3, which yields stable results. The second case uses the same spatial discretization, but does not conform to the temporal Sobolev space properties by using a piecewise constant function for the temporal discretization (Sobolev space order of $-1/2$). This gives an unstable system. The final case uses a correct temporal discretization, but uses a different spatial discretization. In particular, all vector unknowns are expanded with RWG functions, and Eqs. (20) and (23) are tested with RWG functions. Similarly, both scalar unknowns are expanded with piecewise constant functions on primal mesh triangles, and Eqs. (21) and (23) are tested with scalar BC functions. This system is unstable due to the nearly singular matrix that results from discretizing the rotated identity operators in Eqs. (20) and (23).

To demonstrate the stability of the method on a more complicated object, a thin double ogive is simulated. The thin double ogive is generated in two steps. The first step generates a traditional double ogive through a body-of-revolution line defined by

$$\rho(z) = \begin{cases} \dfrac{5f(z)}{1-\cos(46.4^\circ)}, & \text{for} \quad -12.5 < z < 0 \\ \dfrac{5g(z)}{1-\cos(22.62^\circ)}, & \text{for} \quad 0 < z < 25, \end{cases} \tag{30}$$

where

$$f(z) = \sqrt{1-\left(\frac{z}{12.5}\right)^2 \sin^2(46.6^\circ)} - \cos(46.6^\circ), \tag{31}$$

$$g(z) = \sqrt{1-\left(\frac{z}{25}\right)^2 \sin^2(22.62^\circ)} - \cos(22.62^\circ), \tag{32}$$

and all dimensions are in inches. The second step makes the double ogive thin by shrinking all the locations of nodes in the mesh by a factor of 10 along a single dimension. The resulting object is shown in the inset of Fig. 3(b). It is traditionally considered difficult for MOT systems to achieve stability for objects that are thin or have sharp points, making this thin double ogive a good object to test the stability of the method presented in this work.

The simulation parameters for the thin double ogive are the following. The excitation is a plane wave with temporal variation defined by a modulated Gaussian pulse. The center frequency is 15 MHz, the bandwidth is 5 MHz, and the time step is 2.5 ns. The thin double ogive has a relative permittivity of 4 and a relative permeability of 2. Due to the large size of the matrix system, only the largest 5000 eigenvalues are computed for this simulation. These are plotted in Fig. 3(b), which demonstrates the stability of the system.

The next example demonstrates the accuracy of the formulation presented in this work. A one meter radius sphere with a relative permittivity of 1.9 is simulated. The excitation is a plane wave with center frequency of 10 MHz and a bandwidth of 6 MHz. The time step is 3.125 ns. The E-plane bistatic RCS computed from the simulation is compared to an analytical solution in Fig. 4(a), with very good agreement observed.

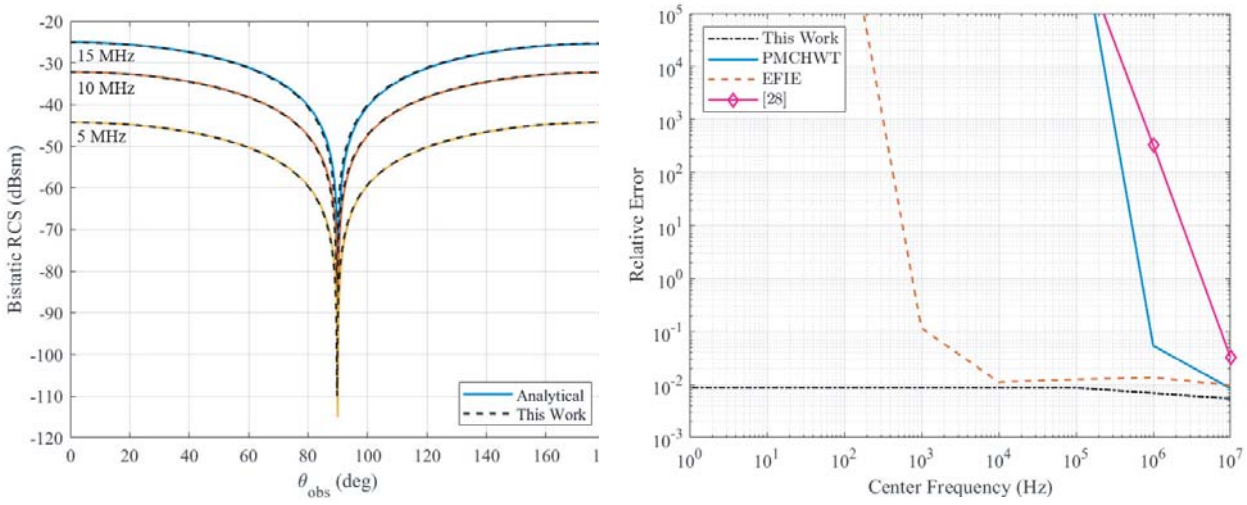

(a) (b)

Figure 4. Accuracy of the formulation developed in this work demonstrated through (a) comparison of analytical and simulated RCS results for a dielectric sphere and (b) error in the RCS at low frequencies for the PMCHWT, EFIE, the formulation of [28], and the formulation of this work.

To demonstrate that the formulation maintains high accuracy down to very low frequencies, a sequence of simulations with center frequencies between 1 Hz to 10 MHz were performed for the one meter radius sphere with relative permittivity of 2.56. For each case, the bandwidth is set to half the center frequency. The error in the bistatic RCS over the E-plane was then computed at the center frequency of each simulation using

$$\text{Error} = \frac{||\text{RCS}_{\text{TDIE}} - \text{RCS}_{\text{Mie}}||}{||\text{RCS}_{\text{Mie}}||}, \tag{33}$$

where $||\cdot||$ is the ℓ_2 norm, RCS_{TDIE} is the RCS calculated using the TDIE, and RCS_{Mie} is the RCS computed with the Mie series (analytical result). The error is plotted in Fig. 4(b), where it is seen that the formulation of this work maintains a high accuracy over the entire range of frequencies considered. Fig. 4(b) also plots the accuracy for standard methods, such as the EFIE and PMCHWT formulations (definitions can be found in [21]), as well as an initial set of potential-based TDIEs developed in the Lorenz gauge [28]. All of the systems except for the one formulated in this work eventually become highly inaccurate, although the reasons for the inaccuracy are different. For the field-based systems, the

inaccuracy comes about because the systems suffer a catastrophic low frequency breakdown, becoming unstable. In the case of the potential-based system from [28], the system loses accuracy but never becomes unstable. The loss of accuracy is due to the incomplete set of boundary conditions used in formulating the integral equation system at low frequencies. This issue does not affect the integral equations formulated in this work because of the complete set of boundary conditions utilized in developing Eqs. (20) to (23).

Unfortunately, simulations of this system at higher frequencies (where wave physics effects become more substantial) were found to be numerically unstable. At this time, the exact reason for instability has not yet been determined. However, for these situations, the system can be easily modified to remove the scalar unknowns and revert to a standard PMCHWT or Müeller formulation. However, it would be preferable for a single TDIE formulation to be stable over the full range of desired frequencies, making this an area of interest for future work.

5. CONCLUSION

This work developed potential-based TDIEs for penetrable regions formulated in the radiation gauge. This can allow for easier coupling into computations applicable to semiclassical and quantum electrodynamics applications. The spatiotemporal Sobolev space properties of the developed TDIEs were discussed, and a discretization that fully conforms to these properties was developed. Numerical results demonstrating the improved stability of this discretization compared to alternative approaches were presented. Additional results illustrating the accuracy of this formulation down to very low frequencies were also shown. Future work can focus on determining efficient preconditioners for these TDIEs, as well as modifications to improve their stability at higher frequencies.

ACKNOWLEDGMENT

This work was supported by NSF ECCS 169195 and the Distinguished Professorship Grant at Purdue University.

This paper describes objective technical results and analysis. Any subjective views or opinions that might be expressed in the paper do not necessarily represent the views of the U.S. Department of Energy or the United States Government.

Sandia National Laboratories is a multimission laboratory managed and operated by National Technology & Engineering Solutions of Sandia, LLC, a wholly owned subsidiary of Honeywell International Inc., for the U.S. Department of Energy's National Nuclear Security Administration under contract DE-NA0003525.

APPENDIX A. INTRODUCTION TO SPATIOTEMPORAL SOBOLEV SPACES

In this appendix, we present a short primer on the spatiotemporal Sobolev spaces used in this work. For more details, the reader is referred to [17] and the references therein.

The spatiotemporal Sobolev spaces used can be viewed as an *ad hoc* set of spaces that naturally arise when attempting to rigorously study the stability properties of TDIEs. In particular, these Sobolev spaces characterize the needed properties of source functions (e.g., charge and current densities) so that the electromagnetic energy produced by the sources remains finite for all time. Although various approaches exist for addressing this problem, the particular approach of interest here is that pioneered for analyzing acoustic TDIEs in [34], which was extended to electromagnetic TDIEs in [35]. These approaches utilize Fourier-Laplace transforms and Parseval's theorem to convert the challenging problem of studying TDIEs into the more approachable problem of carefully analyzing frequency domain integral equations. As a result, the norms that define the spatiotemporal Sobolev spaces used in this work are expressed through the Fourier-Laplace transform.

The foundations of all of these Sobolev spaces lie in those that arise when studying the scalar wave equation. Namely, $H^{\frac{1}{2}}(S)$ and its dual space $H^{-\frac{1}{2}}(S)$, where the S denotes that these spaces are defined over a surface that forms the boundary of some volume [36]. At a high level, the norms that define these Sobolev spaces ensure that the functions contained in them have sufficient continuity properties

to evaluate the various singular integrals that arise in solving integral equations. For example, the norm that defines the space $H^{\frac{1}{2}}(S)$ is [36]

$$||u||_{H^{\frac{1}{2}}(S)} = \left(\int_S |u(\mathbf{r})|^2 dS + \iint \frac{|u(\mathbf{r}) - u(\mathbf{r}')|^2}{R^3} dS dS' \right)^{\frac{1}{2}}. \tag{A1}$$

As alluded to in the main text, functions in $H^{\frac{1}{2}}(S)$ need to have at minimum a linear variation, such as the pyramid function used in the discretization. Functions in $H^{-\frac{1}{2}}(S)$ are less smooth than functions in $H^{\frac{1}{2}}(S)$, as reflected by the difference in the Sobolev space order of the two spaces. An example of a function in $H^{-\frac{1}{2}}(S)$ is a piecewise constant function.

These scalar spaces, in particular $H^{-\frac{1}{2}}(S)$, also find use for specifying the needed properties of vector functions [17, 36]. This typically takes the form of requiring each component of the vector function to be in $H^{-\frac{1}{2}}(S)$, as well as requiring the result of taking a derivative (e.g., a divergence or curl) to be in $H^{-\frac{1}{2}}(S)$. These are the div- and curl-conforming spaces that are sometimes mentioned in the computational electromagnetics literature [24].

With these points in mind, the spatiotemporal Sobolev spaces used in this work can now be defined. The scalar spaces consist of all functions for which

$$||f||^2_{\mathcal{H}^{s_1,s_2}} = \frac{1}{2\pi} \int_{-\infty+i\sigma}^{\infty+i\sigma} |\omega|^{2s_1} ||\tilde{f}(\cdot,\omega)||^2_{H^{s_2}(\omega,S)} d\omega \tag{A2}$$

is finite. In Eq. (A2), a tilde denotes a function is in the frequency domain and σ is a real, positive constant. From Eq. (A2), it is seen that s_1 is related to the temporal regularity of the function, i.e., how many temporal derivatives can be taken before Eq. (A2) is no longer finite. Similarly, s_2 is related to the spatial regularity of the function. In a loose sense, Eq. (A2) can be interpreted as ensuring the combination of energy produced by f at all frequencies is finite. It should be noted that the spatial norm used in the RHS of Eq. (A2) must have an ω-scaling applied to different terms in the standard norm of this space. This is too technical for this level of discussion, but more details can be found in [23].

Similarly, norms can be used to define the spaces $\mathscr{H}^{s_1,s_2}_{\text{div}}$ and $\mathscr{H}^{s_1,s_2}_{\text{curl}}$. These are

$$||\mathbf{f}||^2_{\mathscr{H}^{s_1,s_2}_{\text{div}}} = \frac{1}{2\pi} \int_{-\infty+i\sigma}^{\infty+i\sigma} |\omega|^{2s_1} ||\tilde{\mathbf{f}}(\cdot,\omega)||^2_{H^{s_2}(\text{div},\omega,S)} d\omega, \tag{A3}$$

$$||\mathbf{f}||^2_{\mathscr{H}^{s_1,s_2}_{\text{curl}}} = \frac{1}{2\pi} \int_{-\infty+i\sigma}^{\infty+i\sigma} |\omega|^{2s_1} ||\tilde{\mathbf{f}}(\cdot,\omega)||^2_{H^{s_2}(\text{curl},\omega,S)} d\omega, \tag{A4}$$

where the spatial norms on the RHS of these equations are

$$||\tilde{\mathbf{f}}||_{H^{-\frac{1}{2}}(\text{div},\omega,S)} = \left(||\tilde{\mathbf{f}}||^2_{H^{-\frac{1}{2}}(\omega,S)} + \frac{1}{|\omega|^2} ||\nabla \cdot \tilde{\mathbf{f}}||^2_{H^{-\frac{1}{2}}(\omega,S)} \right)^{\frac{1}{2}}, \tag{A5}$$

$$||\tilde{\mathbf{f}}||_{H^{-\frac{1}{2}}(\text{curl},\omega,S)} = \left(||\tilde{\mathbf{f}}||^2_{H^{-\frac{1}{2}}(\omega,S)} + \frac{1}{|\omega|^2} ||\nabla \times \tilde{\mathbf{f}}||^2_{H^{-\frac{1}{2}}(\omega,S)} \right)^{\frac{1}{2}}. \tag{A6}$$

Similar to Eq. (A2), these norms can be viewed as ensuring the combination of energy produced by $\mathbf{f}$ at all frequencies is finite.

As mentioned in the main text, choosing basis and testing functions that conform to the properties of these Sobolev spaces can significantly improve the accuracy and stability of a discretization. However, it is still possible to arrive at a poorly performing discretization while choosing basis and testing functions from the correct Sobolev spaces. An example of this is the spatial discretization that led to an unstable system in Section 4. Hence, it is also important to supplement the functional analysis that leads to these Sobolev space properties with additional insight. Differential forms and discrete exterior calculus are excellent examples of mathematical formalisms that can complement the Sobolev space analysis to achieve a well-performing discretization [31, 37].

REFERENCES

1. Cohen-Tannoudji, C., J. Dupont-Roc, and G. Grynberg, *Photons and Atoms: Introduction to Quantum Electrodynamics*, Wiley Interscience, 1997.
2. Walls, D. F. and G. J. Milburn, *Quantum Optics*, Springer Science & Business Media, 2007.
3. Liu, A. Y. and W. C. Chew, "Dressed atom fields and dressed states in waveguide quantum electrodynamics," *IEEE Journal on Multiscale and Multiphysics Computational Techniques*, Vol. 2, 58–65, 2017.
4. Rodriguez, A. W., A. P. McCauley, J. D. Joannopoulos, and S. G. Johnson, "Casimir forces in the time domain: Theory," *Physical Review A*, Vol. 80, No. 1, 012115, 2009.
5. Gregersen, N., P. Kaer, and J. Mørk, "Modeling and design of high-efficiency single-photon sources," *IEEE Journal of Selected Topics in Quantum Electronics*, Vol. 19, No. 5, 1–16, 2013.
6. Kandala, A., A. Mezzacapo, K. Temme, M. Takita, M. Brink, J. M. Chow, and J. M. Gambetta, "Hardware-efficient variational quantum eigensolver for small molecules and quantum magnets," *Nature*, Vol. 549, No. 7671, 242–246, 2017.
7. Barends, R., J. Kelly, A. Megrant, A. Veitia, D. Sank, E. Jeffrey, T. C. White, J. Mutus, A. G. Fowler, B. Campbell, et al., "Superconducting quantum circuits at the surface code threshold for fault tolerance," *Nature*, Vol. 508, No. 7497, 500–503, 2014.
8. Shanker, B., A. A. Ergin, M. Lu, and E. Michielssen, "Fast analysis of transient electromagnetic scattering phenomena using the multilevel plane wave time domain algorithm," *IEEE Transactions on Antennas and Propagation*, Vol. 51, No. 3, 628–641, 2003.
9. Yilmaz, A. E., J.-M. Jin, and E. Michielssen, "Time domain adaptive integral method for surface integral equations," *IEEE Transactions on Antennas and Propagation*, Vol. 52, No. 10, 2692–2708, 2004.
10. Chen, N.-W., K. Aygun, and E. Michielssen, "Integral-equation-based analysis of transient scattering and radiation from conducting bodies at very low frequencies," *IEE Proceedings — Microwaves, Antennas and Propagation*, Vol. 148, No. 6, 381–387, 2001.
11. Cools, K., F. P. Andriulli, F. Olyslager, and E. Michielssen, "Time domain Calderón identities and their application to the integral equation analysis of scattering by PEC objects Part I: Preconditioning," *IEEE Transactions on Antennas and Propagation*, Vol. 57, No. 8, 2352–2364, 2009.
12. Qian, Z.-G. and W. C. Chew, "Fast full-wave surface integral equation solver for multiscale structure modeling," *IEEE Transactions on Antennas and Propagation*, Vol. 57, No. 11, 3594–3601, 2009.
13. Taskinen, M. and P. Ylä-Oijala, "Current and charge integral equation formulation," *IEEE Transactions on Antennas and Propagation*, Vol. 54, No. 1, 58–67, 2006.
14. Liu, Q. S., S. Sun, and W. C. Chew, "A potential based integral equation method for low-frequency electromagnetic problems," *IEEE Transactions on Antennas and Propagation*, Vol. 66, No. 3, 1413–1426, 2018.
15. Li, J., X. Fu, and B. Shanker, "Decoupled potential integral equations for electromagnetic scattering from dielectric objects," *IEEE Transactions on Antennas and Propagation*, Vol. 67, No. 3, 1729–1739, 2018.
16. Roth, T. E. and W. C. Chew, "Development of stable A-Φ time domain integral equations for multiscale electromagnetics," *IEEE Journal on Multiscale and Multiphysics Computational Techniques*, Vol. 3, 255–265, 2018.
17. Roth, T. E. and W. C. Chew, "Stability analysis and discretization of A-Φ time domain integral equations for multiscale electromagnetics," *Journal of Computational Physics*, 109102, 2019.
18. Jackson, J. D., *Classical Electrodynamics*, Wiley, 1999.
19. Stratton, J. A., *Electromagnetic Theory*, John Wiley & Sons, 2007.
20. Tai, C.-T., "Direct integration of field equations," *Progress In Electromagnetics Research*, Vol. 28, 339–359, 2000.
21. Jin, J.-M., *Theory and Computation of Electromagnetic Fields*, John Wiley & Sons, 2011.

22. Chew, W. C., *Waves and Fields in Inhomogeneous Media*, IEEE Press, 1995.
23. Ha-Duong, T., "On retarded potential boundary integral equations and their discretisation," *Topics in Computational Wave Propagation*, 301–336, Springer, 2003.
24. Cools, K., F. Andriulli, D. De Zutter, and E. Michielssen, "Accurate and conforming mixed discretization of the MFIE," *IEEE Antennas and Wireless Propagation Letters*, Vol. 10, 528–531, 2011.
25. van'tWout, E., D. R. van der Heul, H. van der Ven, and C. Vuik, "Stability analysis of the marchingon-in-time boundary element method for electromagnetics," *Journal of Computational and Applied Mathematics*, Vol. 294, 358–371, 2016.
26. Bachelot, A., L. Bounhoure, and A. Pujols, "Couplage éléments finis-potentiels retardés pour la diffraction électromagnétique par un obstacle hétérogène," *Numerische Mathematik*, Vol. 89, No. 2, 257–306, 2001.
27. Roth, T. E. and W. C. Chew, "Potential-based TDIEs for dielectric regions using magnetic currents," *2019 IEEE International Symposium on Antennas and Propagation and USNC-URSI Radio Science Meeting*, 1443–1444, IEEE, 2019.
28. Roth, T. E. and W. C. Chew, "Initial potential-based time domain surface integral equations for dielectric regions," *2019 PhotonIcs & Electromagnetics Research Symposium — Spring (PIERS — Spring)*, Rome, Italy, June 17–20, 2019.
29. Buffa, A. and S. Christiansen, "A dual finite element complex on the barycentric refinement," *Mathematics of Computation*, Vol. 76, No. 260, 1743–1769, 2007.
30. Rao, S., D. Wilton, and A. Glisson, "Electromagnetic scattering by surfaces of arbitrary shape," *IEEE Transactions on Antennas and Propagation*, Vol. 30, No. 3, 409–418, 1982.
31. Dai, Q. I., W. C. Chew, L. J. Jiang, and Y. Wu, "Differential-forms-motivated discretizations of electromagnetic differential and integral equations," *IEEE Antennas and Wireless Propagation Letters*, Vol. 13, 1223–1226, 2014.
32. Chen, Q. and D. Wilton, "Electromagnetic scattering by three-dimensional arbitrary complex material/conducting bodies," *International Symposium on Antennas and Propagation Society, Merging Technologies for the 90's*, 590–593, IEEE, 1990.
33. Walker, S., M. Bluck, and I. Chatzis, "The stability of integral equation time-domain scattering computations for three-dimensional scattering; similarities and differences between electrodynamic and elastodynamic computations," *International Journal of Numerical Modelling: Electronic Networks, Devices and Fields*, Vol. 15, No. 5-6, 459–474, 2002.
34. Bamberger, A., T. Ha-Duong, and J. C. Nédélec, "Formulation variationnelle espace-temps pour le calcul par potentiel retardé de la diffraction d'une onde acoustique (I)," *Mathematical Methods in the Applied Sciences*, Vol. 8, No. 1, 405–435, 1986.
35. Terrasse, I., "Résolution mathématique et numérique des équations de Maxwell instationnaires par une méthode de potentiels retardés," Ph.D. dissertation, 1993.
36. Hsiao, G. C. and R. E. Kleinman, "Mathematical foundations for error estimation in numerical solutions of integral equations in electromagnetics," *IEEE Transactions on Antennas and Propagation*, Vol. 45, No. 3, 316–328, 1997.
37. Desbrun, M., E. Kanso, and Y. Tong, "Discrete differential forms for computational modeling," *Discrete Differential Geometry*, 287–324, Springer, 2008.